Effects of freezing, fixation and dehydration on surface roughness properties of porcine left anterior descending coronary arteries

Burton, Hanna; Williams, Richard; Espino, Daniel

DOI:
10.1016/j.micron.2017.06.009

Document Version
Peer reviewed version

Citation for published version (Harvard):
Burton, H, Williams, R & Espino, D 2017, 'Effects of freezing, fixation and dehydration on surface roughness properties of porcine left anterior descending coronary arteries', *Micron*.
https://doi.org/10.1016/j.micron.2017.06.009

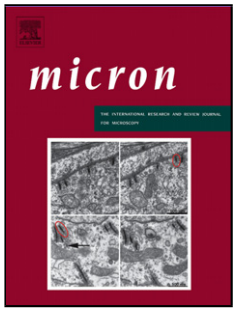

Title: Effects of freezing, fixation and dehydration on surface roughness properties of porcine left anterior descending coronary arteries

Authors: Hanna E. Burton, Richard L. Williams, Daniel M. Espino

PII: S0968-4328(17)30185-3
DOI: http://dx.doi.org/doi:10.1016/j.micron.2017.06.009
Reference: JMIC 2446

To appear in: *Micron*

Received date: 27-4-2017
Revised date: 15-6-2017
Accepted date: 19-6-2017

Please cite this article as: Burton, Hanna E., Williams, Richard L., Espino, Daniel M., Effects of freezing, fixation and dehydration on surface roughness properties of porcine left anterior descending coronary arteries.Micron http://dx.doi.org/10.1016/j.micron.2017.06.009

Effects of freezing, fixation and dehydration on surface roughness properties of porcine left anterior descending coronary arteries

Hanna E. Burton[a, b] (hem344@bham.ac.uk)

Richard L. Williams[b] (r.l.williams.2@bham.ac.uk)

Daniel M. Espino[a]* (d.m.espino@bham.ac.uk)

[a] Biomedical Engineering Research Group, Department of Mechanical Engineering, University of Birmingham, B15 2TT, United Kingdom

[b] School of Chemical Engineering, University of Birmingham, B15 2TT, United Kingdom

*Corresponding author:

Daniel M. Espino
Department of Mechanical Engineering
University of Birmingham
United Kingdom
B15 2TT
Tel.: +44 (0) 121 414 7355
Fax: +44 (0) 121 414 3958
Email address: d.m.espino@bham.ac.uk

Highlights

- Freeze-thaw effect on physical dimensions and surface roughness of coronary artery
- Processing (fixation and dehydration) of coronary arteries for microscopic imaging
- Surface roughness measurements assess changes during processing of tissue
- Correction factor accounting for processing of soft biological tissue

Abstract

Background: To allow measurements of surface roughness to be made of coronary arteries using various imaging techniques, chemical processing, such as fixation and dehydration, is commonly used. Standard protocols suggest storing fresh biological tissue at -40°C. The aim of this study was to quantify the changes caused by freezing and chemical processing to the surface roughness measurements of coronary arteries, and to determine whether correction factors are needed for surface roughness measurements of coronary arteries following chemical processes typically used before imaging these arteries.

Methods: Porcine left anterior descending coronary arteries were dissected *ex vivo*. Surface roughness was then calculated following three-dimensional reconstruction of surface images obtained using an optical microscope. Surface roughness was measured before and after a freeze cycle to assess changes during freezing, after chemical fixation, and again after dehydration, to determine changes during these steps of chemical processing.

Results: No significant difference was caused due to the freeze cycle ($p > 0.05$). There was no significant difference in the longitudinally measured surface roughness (Ra_L = 0.99 ± 0.39 µm; $p > 0.05$) of coronary arteries following fixation and dehydration either. However, the circumferentially measured surface roughness increased significantly following a combined method of processing (Ra_C = 1.36 ± 0.40, compared 1.98 ± 0.27 µm, respectively; $p < 0.05$). A correction factor can compensate for the change in Ra_C due to processing of tissue, $Ra_{C\beta} = \frac{Ra_C}{1+0.46}$. Where $Ra_{C\beta}$, the corrected Ra_C, had a mean of 1.31 ± 0.21 µm.

Conclusions: Independently, freezing, fixation and dehydration do not alter the surface roughness of coronary arteries. Combined, however, fixation and dehydration significantly increase the circumferential, but not longitudinal, surface roughness of coronary arteries.

Keywords: Coronary arteries; Dehydration; Fixation; Freezing; Surface imaging; Surface roughness

1 Background

Coronary heart disease, a result of coronary artery disease, is the leading cause of death worldwide (1). In the USA it was the underlying cause of death in 1 out of every 7 deaths in 2011, and associated direct and indirect costs were estimated to be $204.4 billion in 2010 (2). The gold standard practice for artery replacement is to use the patients' own artery or vein as a graft (3), however, 30-40% of patients lack a viable vein (4). The development of biomaterials can aid in creating a feasible alternative (5). For instance, restenosis following angioplasty occurs within 3-6 months for 40-50% of patients, but decreases with stenting to 20-30% (6). While this is an improvement, there is a push to develop novel stents to increase endothelialisation but also to prevent restenosis and thrombus formation (7, 8).

Progress has been made in developing suitable bulk materials for coronary artery replacement (9), but surface properties have received less attention. Surface modification, however, allows the bulk modulus of the material to remain unchanged but with the additional benefit of being able to: increase the biocompatibility of materials (10-14); influence cell growth, alignment, viability and attachment (15-24), and increase patency rates by deterring thrombus formation (7, 12, 25). However, replication of bio-inspired surface texturing requires measurements of the physical properties of surfaces.

Surface properties of materials, and topography, are typically characterised through their mean surface roughness, *Ra*, the arithmetic average of absolute values of sampling length (26). While surfaces of coronary arteries have been analysed qualitatively (27), the feasibility of quantitatively measuring the surface roughness has only recently been established (28). *Ra* was calculated from three dimensional reconstructed optical images of porcine left anterior descending (LAD) coronary arteries. Beyond providing a standard for surface roughness of replacement materials, surface roughness may also have applications to identify disease; recent examples include assessment of diabetics' red blood cells (29) and grading of osteoarthritis in cartilage (30).

The preparation of biological tissues for microscopy typically requires various procedures, including freezing, fixation and dehydration. The effect of these procedures on certain physical characteristics of tissues are known, and can be accounted for, including changes in dimensions of the heart (31) and biological tissue (32), and correcting cell density of endothelium (33). Currently, however, it is unknown whether *Ra* might be altered by preparatory procedures used for soft connective tissues (such as coronary arteries).

The aim of this study was to quantify the surface roughness (*Ra*) of porcine LAD coronary arteries, through optical microscopy. Furthermore, to determine whether freezing, fixation and dehydration, common procedures for preparing biological specimens for microscopy (e.g. Scanning Electron Microscopy, SEM) alter the measured *Ra*; and if so, to determine a suitable correction factor. Porcine hearts are an established model of human hearts due to their anatomical similarity (34, 35), and were therefore chosen for use in this study.

2 Methods

2.1 Specimens

Six porcine hearts were obtained from Fresh Tissue Supplies (Horsham, UK), and frozen on excision. No animals were sacrificed specifically for this study. Ethical approval was granted for this study by

the University of Birmingham *Research Support Group* [ERN_15-0032]. Hearts were wrapped in tissue paper soaked in Ringer's solution and stored at -40°C. Before dissection hearts were defrosted at 4 °C overnight. The LAD coronary artery was identified and dissected from the most distal point visible to the bifurcation of the LAD and the left circumflex coronary artery (LCX). A longitudinal incision (along the length of the artery) was made along the LAD sample so as to expose its internal surface (Figure 1), with excess tissue removed. Finally, the sample was sectioned into three specimens of 20 mm each leading to 18 tissue samples. These tissue samples were categorised as proximal, middle and distal where in this case proximal refers to a position nearer the base of the heart and distal near to the apex of the heart, along a longitudinal axis of the LAD (Figure 1). For consistency, the six middle tissue samples were used in this study; however, the *Ra* of porcine LAD coronary arteries does not differ along its length (28). Tissue samples were wrapped in tissue paper soaked in Ringer's solution and stored at -40 °C until required for microscopy. Before further testing, tissue samples were defrosted at 4 °C for an hour, following protocols from previous studies of porcine heart tissue (36-39).

Dimensions of tissue samples were measured using a Vernier calliper at each stage of tissue processing. For each individual specimen (n = 6), the mean of three measurements was taken for length (L), width at either end of the specimen (W_1 and W_2 respectively), and thickness (t) of specimens (Figure 1). Measurement of these dimensions were repeated at each stage of imaging of the specimens (Figure 2).

2.2 Optical imaging

An optical focus variation microscope (G5 Infinite Focus , Alicona UK, Kent, UK) was used to image the surface of the specimens at 10× magnification (10× Nikon CFI 60 TU Plan Epi Infinity Corrected Obj lens, Alicona UK, Kent, UK), as described previously (28). The Alicona Infinite Focus (IF) microscope is a non-contact, optical, three-dimensional (3D) measurement system. Lighting was controlled via white LED (Light Emitting Diode) coaxial illumination. Illumination intensity, and lateral (X and Y axis) and vertical (Z axis) resolution were adjusted using automated ideal settings, as defined using the instruments' software, Alicona IF-Measure Suite (version 5.1, Alicona UK, Kent, UK), consistent with previous studies (40). The Alicona software was used to obtain and analyse all images.

Briefly, imaging was performed at four stages in this study (Figure 2): before and after a freeze-thaw cycle; following fixation; and following dehydration. A three-dimensional reconstruction of the image was performed using the Alicona IF-Laboratory Measurement Module (version 6.1, Alicona UK, Kent, UK), from which the *Ra* was measured. The three-dimensional reconstruction process is described elsewhere (28). Briefly, the entire surface of each sample was imaged and reconstructed. Subsequently, five profile lengths with a mean of 2.63 ± 0.67 mm were measured along two directions aligned with circumferential and longitudinal sample orientations (Figure 1). The *Ra* was assessed both longitudinally and circumferentially, as previously a significant difference was found between the two orientations (28). When measuring *Ra* profiles, bifurcations where smaller vessels connected to the LAD were avoided during profile selection. They were avoided because they formed part of the blood vessel structure rather than being an intrinsic property of the surface. Also, profiles were not measured near the edges of the sample where distortion may have occurred during dissection. Equation 1 and Equation 2 (41) were used to calculate surface roughness in the circumferential direction, RaC, and the longitudinal direction, RaL, respectively.

Equation 1

$$Ra_C = \frac{1}{l}\int_0^l |Z(x)|dx$$

Equation 2

$$Ra_L = \frac{1}{l}\int_0^l |Z(y)|dy$$

Where Z(x) is the profile height function along x (Equation 1), Z(y) is profile height function along y (Equation 2), and l is the sampled length. The mean surface roughness for each individual specimen (n = 6) was determined from five repeat measurements taken in each direction.

2.3 Tissue preparation

Tissue samples underwent fixation and dehydration, following a standard protocol for soft mammalian tissues (42). Briefly, specimens were immersed in a 3% glutaraldehyde solution (Fluka Analytical, Sigma Aldrich, St Louis, MO, USA) with 0.2 M sodium phosphate buffer for 1 hour, at an average pH value for animal tissue of pH 7.4 (43) (Table 1). Subsequently, specimens were rinsed in three 10 minute washes of phosphate buffer saline (PBS) solution to remove any remaining glutaraldehyde. To ensure that the samples remained hydrated they were stored in PBS solution at 4°C until dehydration.

Dehydration was performed in washes of 10 minutes with increasing concentrations of ethanol (Fisher Chemical, Fisher Scientific UK Ltd, Loughborough, UK) at 30%, 50%, 70%, 95% and two washes at 100%. The concentration series ensures that dehydration occurs in a controlled manner, minimising distortion of the specimen (32). Finally, hexamethyldisilazane (HMDS; Aldrich Chemistry, St Louis, MO, USA) was used to complete dehydration (44), removing any remaining ethanol from the specimen by displacement. The specimen underwent a wash of HMDS for 15 minutes before replenishing with fresh HMDS to be left overnight to evaporate.

2.4 Correction Factor

A correction factor was calculated for *Ra* when a significant difference was identified following processing. Ra_β, a corrected surface roughness value, was calculated using Equation 3.

Equation 3

$$Ra_\beta = \frac{Ra}{1 - \alpha}$$

α was calculated using Equation 4, where Ra_{pre} and Ra_{post} were the mean values of *Ra* before and after processing respectively.

Equation 4

$$\alpha = \frac{Ra_{pre} - Ra_{post}}{Ra_{pre}}$$

2.5 Data analysis

All statistical analysis was performed using Minitab Statistical Software (Minitab 17.0, Minitab Inc, State College, PA, USA). To assess the effect of a freeze cycle (Figure 2; stages 1 and 2) on surface roughness and physical dimensions on coronary arteries, a student paired *t-test* ($p < 0.05$) was performed for each dependent variable (Ra_C, Ra_L, L, W_1 and W_2) (45).

A one-way repeated measures Multivariance Analysis of Variance (MANOVA) test was performed to analyse processing of coronary arteries (Figure 2), and to assess whether there was a significant difference in surface roughness and physical dimensions of the tissue (45, 46). Multiple dependent variables (Ra_C, Ra_L, L, W_1 and W_2) were compared during three independent stages (Figure 2; stages 1, 3 and 4), with the risk of Type 1 errors reduced due to the choice of MANOVA (47). If a statistical significance was identified ($p < 0.05$) using a MANOVA test, Analysis of Variance (ANOVA) was then performed on each dependent variable using Tukey's method ($p < 0.05$) to determine which stage of the independent variable resulted in this change. When a correction factor was applied to results, a student paired *t-test* was performed between the calculated and actual results to determine if there was a significant difference ($p < 0.05$).

3 Results

3.1 Surface Roughness

Figure 3 shows the 3D reconstructed surface at each stage of processing, with the respective optical images shown in Figure 4. Sample *Ra* profiles aligned circumferentially and longitudinally along the LAD coronary artery are provided in Figure 5. From these figures an increased surface roughness in the circumferential over longitudinal direction can be observed, with ridges visible (Figures 3 and 4).

Ra_C values ranged from 0.82 to 2.26 µm. Freezing (1.28 ± 0.34 µm), fixation (1.49 ± 0.49 µm) and dehydration (1.98 ± 0.26 µm), independently, did not significantly alter Ra_C ($p > 0.05$; Table 2) from one stage of tissue preparation to the next. However, the cumulative effect of fixation and dehydration during the preparation stages led to a significant increase in Ra_C from 1.36 ± 0.27 µm (the initial surface roughness) to 1.98 ± 0.26 µm ($p < 0.05$;Table 2) following all tissue preparation (Figure 6).

Ra_L measurements ranged from 0.57 to 2.24 µm. Freezing (1.00 ± 0.38 µm), fixation (1.03 ± 0.55 µm) and dehydration (1.07 ± 0.18 µm), independently, did not significantly alter Ra_L ($p > 0.05$;Table 2; Figure 6). There was no significant difference in the initial Ra_L (0.87 ± 0.30 µm) and that measured following the cumulative effect of freezing, fixation and dehydration (1.07 ± 0.18 µm; $p > 0.05$; Table 2; Figure 6).

3.2 Ra correction factor

Ra_C was significantly increased following processing, thus a correction factor was applied. The correction factor, α, calculated using Equation 5 was -0.46, was inserted into Equation 3 to calculate $Ra_{C\beta}$, the corrected surface roughness in the circumferential direction, as shown in Equation 5.

Equation 5

$$Ra_{C\beta} = \frac{Ra_C}{1 + 0.46}$$

The mean Ra_{C6} was 1.31 ± 0.21 µm. No significant difference was found between the original Ra_C values and the calculated Ra_{C6} values ($p > 0.05$; Table 2).

3.3 Tissue dimensions

Freezing did not significantly alter any of the physical dimensions ($p > 0.05$; Table 2); the physical dimensions of tissue, though, were significantly altered due to the cumulative effect of processing ($p < 0.01$;Table 2). The initial length of specimens (1.98 ± 0.11 mm) was not significantly different to the fixed specimen lengths (1.83 ± 0.13 mm, $p > 0.05$), but they were significantly greater than the dehydrated specimen lengths (1.56 ± 0.44 mm, $p = 0.001$; Table 2). The fixed lengths were also significantly greater than the dehydrated lengths ($p < 0.05$; Table 2).

The initial width at W_1 and W_2 (0.71 ± 0.07 and 0.58 ± 0.08 mm, respectively) were significantly greater than the widths after processing (0.55 ± 0.08 and 0.43 ± 0.06 mm, W_1 and W_2 respectively, $p < 0.05$; Table 2). However, the individual stages of fixation (0.62 ± 0.05 and 0.53 ± 0.06 mm, W_1 and W_2 respectively) and dehydration caused no significant differences to the width measurements ($p > 0.05$; Table 2). The thickness of specimens ranged from 0.02 to 0.05 mm. No significant difference was seen in thickness due to the processing stages ($p > 0.05$; Table 2).

4 Discussion

This study has investigated the effects caused by freezing and chemical processing of connective tissues on the surface roughness and physical dimensions of LAD coronary arteries. The procedure of preparing LAD coronary artery samples for microscopy (i.e. freezing, glutaraldehyde-fixation, and dehydration) led to the cumulative effect of tissue shrinkage and increased circumferential surface roughness. The dehydration process caused the most significant change to values, and this was obvious when looking at the cumulative effect of processing, as fixing alone did not cause any changes. Ra_L was not significantly affected by the processing, however, Ra_C was more sensitive to the processing and a correction factor was developed for this (Equation 5). Further, Equations 3 and 4 provide a generalised description for developing correction factors for *Ra* of soft connective tissues.

Freezing alone did not affect the surface roughness or physical dimensions of samples. Storage via freezing is a standard protocol employed by many studying biological tissue (36, 38, 48, 49). Freezing prevents the degradation of biological tissues which require storage (49). Minimal changes have been noted of the biomechanical properties due to repeat freeze-thaw cycles of soft tissue allografts (50), or prolonged freeze storage of porcine aortic tissue (48). While other studies have noted that any effects of freezing soft connective tissues are outweighed by the standard deviation of the original measurements (51). The results in this study confirm that soft connective tissues stored at -40°C are not altered in physical dimensions; further, that this storage procedure does not affect the surface roughness (*Ra*) of coronary arteries.

Previous studies have highlighted the benefits of storing tissue cryogenically with an appropriate cryo-protectant (52) to allow indefinite storage of blood vessels. Additionally, without the use of a cryo-protectant, when storing tissues at -20 °C, the stress-strain properties of porcine femoral arteries were altered; potentially due to ice crystal growth or damage to the extracellular matrix (53). However, storing soft tissues at -20 °C has revealed no changes in mechanical properties for porcine liver (54), porcine aortic samples (48) and murine tendons (49) to name but a few. Increased rate of storage and lower storage temperature are known to reduce of the size ice-crystals (55), with smaller ice-crystals having less effect on the extra-cellular matrix composing soft connective tissues

(56). In this study, a protocol for storing soft tissues by freezing at -40 °C was used (13-16). Further, neither repeated freeze–thaw cycles or extended frozen storage have been found to lead to more than minimal changes in biomechanical properties, for bone-patella tendon-bone soft tissue allografts (50) and porcine aortic tissue (48), respectively. This is consistent with our own finding that a freeze-thaw cycle did not alter surface roughness of the tissue at -40 °C. Although no significant difference was seen in surface roughness after a freeze-thaw cycle, some established storage procedures do incorporate cryo-storage and cryo-protectants (52, 57, 58). Therefore, it would be of value to assess the effect of cryo-protectants on the surface roughness of soft connective tissues using the methodology from this current study.

Arteries are made up of smooth muscle cells, collagen, and elastin (59, 60). Fixation is used to preserve the structure of the samples and prevent degradation of connective tissues, through the reacting of aldehyde groups (61) in the fixing solution (e.g. glutaraldehyde) with amino acids found in collagen (62), forming crosslinks between the collagen fibres (43, 63, 64). Conversely, elastin is not fixed by glutaraldehyde or formaldehyde fixatives (65). Glutaraldehyde is often chosen for fixation to attempt to preserve the mechanical properties of tissue (66), preventing their degradation during storage for instance. However, the cross-linking process is known to affect the anisotropy of biological materials such as pericardium tissue (67), with an increase in mechanical strength seen in pulmonary ligaments (68) and increase in elasticity noted elsewhere in pericardial tissue (69). Conversely, heart valve tissue was found to be less stiff following fixation (70). Regardless, fixation affects the structure and mechanical strength of tissue. The results of this study determined that the surface roughness was not affected by the fixation procedure; however, it is unclear whether the cross-linking of proteins would be expected to alter the surface roughness of an endothelium lined coronary artery. Dehydration prevents the distortion of light when performing microscopy and is necessary to ensure a vacuum for traditional SEM for instance (43, 71). Biological tissue in the human body is naturally hydrated, and the dehydration of tissue has been shown to affect its viscoelastic properties (72, 73). The dehydration process removes both free water molecules, and those bound to the tissue such as water soluble proteins. Therefore, the results of this study which show that both the circumferential surface roughness and physical dimensions of coronary arteries are significantly altered due to dehydration appear reasonable. Further, the dependency of tissue dimensions on hydration, and the finding in this study that surface roughness changed significantly only subsequent to dehydration, imply that the need for a correction factor to compensate for the changes due to processing should be considered particularly when tissue processing includes dehydration.

The correction factor in this study can be used as a standard for preparing coronary artery tissue through fixation and dehydration. This correction factor would provide outer limits of the circumferential surface roughness measurements, analogous to how the tissue fraction effect is corrected for in dynamic imaging (74). A correction factor would be beneficial for assessing the effect that processing techniques have on surface roughness measurements of biological tissues. It is accepted that measurements of tissue dimension (31), tumour volume (75), and cell density (33) should be corrected due to the effect of processing, however, this correction has not been quantified previously for surface roughness. The results of this study are beneficial to the development of biomaterials, where replicating the endothelium could be achieved through surface modification techniques, including nano-texturing. This would leave the bulk modulus of the material unchanged, but allow the opportunity to influence cell formation (15-24), increase patency rates (7, 12, 25), and increase biocompatibility (10-14).

This study used glutaraldehyde based fixation, typically associated with the preparation of samples for SEM. This assessment is of value because it is difficult to perform SEM on tissues without any preparation, i.e. to obtain a baseline measurement for comparison. Therefore, the correction factor calculated in this paper would be suitable when using the stated protocols when preparing samples for investigation by SEM. Our study, however, has used light microscopy which is typically associated with fixatives such formalin or paraformaldehyde (76, 77). Given that such fixatives tend to be milder as compared to glutaraldehyde fixation, they would not be expected to alter surface roughness. Pointedly, though, the methods proposed in this study could be replicated to assess the effect of a range of fixation (e.g. formalin, paraformaldehyde, etc) and/or dehydration protocols on surface roughness. The methods proposed also enable the need for correction factor to be determined, for a range of soft connective tissues being evaluated for surface roughness.

The correction factor calculated in this paper is similar to that calculated in previous work (28), where α was -0.63 compared to -0.46 found in this study. The variation in values is likely due to the natural variation of biological tissue. The average mean corrected value of $Ra_{C\beta}$ in the previous paper was 1.04 ± 0.47 µm, which is comparable to the value of 1.31 ± 0.21 µm found in this study. A change in *Ra* after processing was only noted in the circumferential direction. Collagen is orientated circumferentially within the thicker medial layer, but axially in the thin sub-endothelial layer; hence a change in surface roughness circumferentially may be due to the collagen within the thicker medial layer causing a significant distortion during fixation compared to axially (78).

The uncorrected Ra_C and Ra_L values (1.98 ± 0.27 µm and 0.99 ± 0.39 µm, respectively) within this paper are comparable to those measured previously (1.69 ± 0.75 µm and 0.89 ± 0.27 µm, respectively) (28). This confirms the repeatability of results, and emphasises the importance of using a correction factor for the circumferential surface roughness. Similar to the previous study, the uncorrected Ra_C was significantly greater than Ra_L.

Coronary arteries are anisotropic, where mechanical properties vary from the longitudinal to circumferential direction. The results in this study, and the authors' previous work (28), now suggest that their surface roughness is too, with the surface roughness of LAD coronary arteries being significantly higher in the circumferential than longitudinal direction. This may have implications for recent studies investigating the helical flow in coronary arteries (79), and potentially multiscale analysis of such flow (80). The main factor in the anisotropy of surface roughness appeared to be the presence of ridges along the artery. These ridges may depend on the underlying arrangement of macro-molecules such as collagen (81) and their orientation in arteries (82-84), and/or may impact on the endothelial cell orientation along the arteries (85). Further investigation into the multi-scale characteristics of the surface roughness of coronary arteries would be beneficial, as *Ra* is dependent on the measurement method used (86). A correction factor could be determined for scanning electron microscopy, to correct the changes caused by processing to surface roughness at a nano-scale. An environmental scanning electron microscope would be useful in aiding this, as it would be possible to measure the surface roughness at the various stages of processing, including in a hydrated form, at higher magnifications than possible with an optical microscope.

5 Conclusions

The findings from this study are as follows:

- a freeze cycle at -40 °C does not significantly alter the surface roughness measurement or physical dimensions of porcine LAD;

- the cumulative process of glutaraldehyde based fixation followed by dehydration, caused no significant difference to Ra_L of porcine LAD, measuring an average mean of 0.99 ± 0.39 µm;
- the cumulative process of glutaraldehyde based fixation followed by dehydration, caused a significant increase to Ra_C, from 1.36 ± 0.40 to 1.98 ± 0.27 µm
- changes to surface roughness due to processing of tissue, as described by this paper, can be accounted for by applying the following correction factor:

$$Ra_{C\beta} = \frac{Ra_C}{1 + 0.46}$$

- corrected $Ra_{C\beta}$ has an average mean of 1.31 ± 0.21 µm

In conclusion, while individual preparation procedures of tissues for microscopy may not individually alter the surface roughness of coronary arteries, additive effects may be present (particularly following dehydration) which may require a correction factor. For coronary arteries this is the case circumferentially, but not longitudinally.

Declaration of interest

The authors declare that they have no conflict of interest.

Acknowledgments

HEB is funded by an Engineering and Physical Sciences Research Council scholarship [M114612B]. This study was partly funded by an *Innovation and Research Award* from the *Institute of Physics and Engineering in Medicine*.

References

1. Townsend N, Bhatnagar P, Wilkins E, Wickramasinghe K, Rayner M. Cardiovascular disease statistics, 2015. London: British Heart Foundation; 2015.

2. Mozaffarian D, Benjamin EJ, Go AS, Arnett DK, Blaha MJ, Cushman M, et al. Heart disease and stroke statistics-2015 update: a report from the american heart association. Circulation. 2015;131(4):e29.

3. Chlupac J, Filova E, Bacakova L. Blood vessel replacement: 50 years of development and tissue engineering paradigms in vascular surgery. Physiological Research. 2009;58:S119.

4. Faries PL, LoGerfo FW, Arora S, Pulling MC, Rohan DI, Akbari CM, et al. Arm vein conduit is superior to composite prosthetic-autogenous grafts in lower extremity revascularization. Journal of Vascular Surgery. 2000;31(6):1119-27.

5. Chen Q, Liang S, Thouas GA. Elastomeric biomaterials for tissue engineering. Progress in Polymer Science. 2013;38(3-4):584-671.

6. Lacin NT, Utkan GG. Role of biomaterials in prevention of in-stent restenosis. J Biomedical Materials Research Part B: Applied Biomaterials. 2014;102(5):1113-20.

7. O'Brien B, Carroll W. The evolution of cardiovascular stent materials and surfaces in response to clinical drivers: a review. Acta Biomaterialia. 2009;5(4):945-58.

8. Martinez AW, Chaikof EL. Microfabrication and nanotechnology in stent design. Wiley Interdisciplinary Reviews Nanomedicine Nanobiotechnology. 2011;3(3):256-68.

9. Desai M, Seifalian AM, Hamilton G. Role of prosthetic conduits in coronary artery bypass grafting. European Journal of Cardio-Thoracic Surgery. 2011;40(2):394-8.

10. Liu X, Chu P, Ding C. Surface modification of titanium, titanium alloys, and related materials for biomedical applications. Materials Science and Engineering: R: Reports. 2004;47(3-4):49-121.

11. Kurella A, Dahotre NB. Review paper: surface modification for bioimplants: the role of laser surface engineering. Journal of Biomaterials Applications. 2005;20(1):5-50.

12. Govindarajan T, Shandas R. A survey of surface modification techniques for next-generation shape memory polymer stent devices. Polymers. 2014;6(9):2309-31.

13. Zhao T, Li Y, Xia Y, Venkatraman SS, Xiang Y, Zhao X. Formation of a nano-pattering NiTi surface with Ni-depleted superficial layer to promote corrosion resistance and endothelial cell-material interaction. Journal of Materials Science: Materials in Medicine. 2013;24(1):105-14.

14. Leszczak V, Popat KC. Improved in vitro blood compatibility of polycaprolactone nanowire surfaces. ACS Applied Mmaterials & Interfaces. 2014;6(18):15913-24.

15. Ross AM, Lahann J. Surface engineering the cellular microenvironment via patterning and gradients. Journal of Polymer Science Part B: Polymer Physics. 2013;51(10):775-94.

16. He W, Yong T, Ma ZW, Inai R, Teo WE, Ramakrishna S. Biodegradable polymer nanofiber mesh to maintain functions of endothelial cells. Tissue Engineering. 2006;12(9):2457-66.

17. He W, Ma Z, Yong T, Teo WE, Ramakrishna S. Fabrication of collagen-coated biodegradable polymer nanofiber mesh and its potential for endothelial cells growth. Biomaterials. 2005;26(36):7606-15.

18. Kiyan Y, Kurselis K, Kiyan R, Haller H, Chichkov BN, Dumler I. Urokinase receptor counteracts vascular smooth muscle cell functional changes induced by surface topography. Theranostics. 2013;3(7):516.

19. Le X, Poinern GE, Ali N, Berry CM, Fawcett D. Engineering a biocompatible scaffold with either micrometre or nanometre scale surface topography for promoting protein adsorption and cellular response. International Journal of Biomaterials. 2013;2013:782549.

20. Flemming RG, Murphy CJ, Abrams GA, Goodman SL, Nealey PF. Effects of synthetic micro- and nano-structured surfaces on cell behavior. Biomaterials. 1999;20(6):573-88.

21. Karagkiozaki V, Karagiannidis PG, Kalfagiannis N, Kavatzikidou P, Patsalas P, Georgiou D, et al. Novel nanostructured biomaterials: implications for coronary stent thrombosis. International Journal of Nanomedicine. 2012;7:6063.

22. Fioretta ES, Fledderus JO, Burakowska-Meise EA, Baaijens F, Verhaar MC, Bouten CVC. Polymer-based scaffold designs for in situ vascular tissue engineering: controlling recruitment and differentiation behavior of endothelial colony forming cells. Macromolecular Bioscience. 2012;12(5):577-90.

23. Vartanian KB, Kirkpatrick SJ, Hanson SR, Hinds MT. Endothelial cell cytoskeletal alignment independent of fluid shear stress on micropatterned surfaces. Biochem Biophys Res Commun. 2008;371(4):787-92.

24. Vartanian KB, Kirkpatrick SJ, McCarty OJ, Vu TQ, Hanson SR, Hinds MT. Distinct extracellular matrix microenvironments of progenitor and carotid endothelial cells. Journal of Biomedical Materials Research Part A. 2009;91(2):528-39.

25. DePalma VA, Baier RE, Ford JW, Gott VL, Furuse A. Investigation of three-surface properties of several metals and their relation to blood compatibility. Journal of Biomedical Materials Research. 1972;6(4):37-75.

26. Solouk A, Cousins BG, Mirzadeh H, Solati-Hashtjin M, Najarian S, Seifalian AM. Surface modification of POSS-nanocomposite biomaterials using reactive oxygen plasma treatment for cardiovascular surgical implant applications. Biotechnology and Applied Biochemistry. 2011;58(3):147-61.

27. Bertazzo S, Gentleman E, Cloyd KL, Chester AH, Yacoub MH, Stevens MM. Nano-analytical electron microscopy reveals fundamental insights into human cardiovascular tissue calcification. Nature Materials. 2013;12(6):576-83.

28. Burton HE, Freij JM, Espino DM. Dynamic viscoelasticity and surface properties of porcine left anterior descending coronary arteries. Cardiovascular Engineering and Technology. 2017;8(1):41-56.

29. Buys AV, Van Rooy M-J, Soma P, Van Papendorp D, Lipinski B, Pretorius E. Changes in red blood cell membrane structure in type 2 diabetes: a scanning electron and atomic force microscopy study. Cardiovascular Diabetology. 2013;12(1):25.

30. Peng Z, Wang M. Three dimensional surface characterization of human cartilages at a micron and nanometre scale. Wear. 2013;301(1):210-7.

31. Hołda MK, Klimek-Piotrowska W, Koziej M, Piątek K, Hołda J. Influence of different fixation protocols on the preservation and dimensions of cardiac tissue. Journal of Anatomy. 2016.

32. Bucher D, Scholz M, Stetter M, Obermayer K, Pflüger H-J. Correction methods for three-dimensional reconstructions from confocal images: I. Tissue shrinking and axial scaling. Journal of Neuroscience Methods. 2000;100(1):135-43.

33. Doughty MJ. Correcting cell density measurements for tissue hydration changes in scanning electron microscopy—application to the rabbit corneal endothelium. Tissue and Cell. 1995;27(2):207-20.

34. Ozolanta I, Tetere G, Purinya B, Kasyanov V. Changes in the mechanical properties, biochemical contents and wall structure of the human coronary arteries with age and sex. Medical Engineering & Physics. 1998;20(7):523-33.

35. Van Andel CJ, Pistecky PV, Borst C. Mechanical properties of porcine and human arteries: Implications for coronary anastomotic connectors. Annals of Thoracic Surgery. 2003;76(1):58-64.

36. Millard L, Espino DM, Shepherd DET, Hukins DWL, Buchan KG. Mechanical properties of chordae tendineae of the mitral heart valve: Young's modulus, structural stiffness, and effects of aging. Journal of Mechanics in Medicine and Biology. 2011;11(01):221-30.

37. Espino DM, Shepherd DET, Buchan KG. Effect of mitral valve geometry on valve competence. Heart and Vessels. 2007;22(2):109-15.

38. Espino DM, Hukins DWL, Shepherd DET, Watson MA, Buchan K. Determination of the pressure required to cause mitral valve failure. Medical Engineering & Physics. 2006;28(1):36-41.

39. Espino DM, Shepherd DET, Hukins DW, Buchan KG. The role of chordae tendineae in mitral valve competence. Journal of Heart Valve Disease. 2005;14(5):603-9.

40. Hiersemenzel F, Petzing JN, Leach RK, Helmli F, Singh J. Areal texture and angle measurements of tilted surfaces using focus variation methods. In: Proceedings of the 3rd International Conference on Surface Metrology. Annecy, France, 2012.

41. ISO E. 4287: 2009. Geometrical product specifications (GPS)-surface texture: profile method–terms, definitions and surface texture parameters (ISO 4287: 1997+ Cor 1: 1998+ Cor 2: 2005+ Amd 1: 2009)(includes Corrigendum AC: 2008 and Amendment A1: 2009).

42. Beck SF. Electrón microscopy: a handbook of techniques for the biologist: Nassau Community College; 1998.

43. Hayat MA. Principles and techniques of electron microscopy. London, United Kingdom: Edward Arnold; 1981.

44. Moran P, Coats B. Biological sample preparation for SEM imaging of porcine retina. Microscopy Today. 2012;20(02):28-31.

45. Bland M. An introduction to medical statistics: Oxford University Press; 2000.

46. Reilly J. Applied statistics: Statistical Solutions; 2015. Available from: www.statisticalsolutions.ie.

47. Bock RD. Multivariate statistical methods in behavioral research: Scientific Software International; 1975.

48. O'Leary SA, Doyle BJ, McGloughlin TM. The impact of long term freezing on the mechanical properties of porcine aortic tissue. Journal of the Mechanical Behavior of Biomedical Materials. 2014;37:165-73.

49. Goh KL, Chen Y, Chou SM, Listrat A, Bechet D, Wess TJ. Effects of frozen storage temperature on the elasticity of tendons from a small murine model. Animal. 2010;4(9):1613-7.

50. Jung HJ, Vangipuram G, Fisher MB, Yang G, Hsu S, Bianchi J, et al. The effects of multiple freeze-thaw cycles on the biomechanical properties of the human bone-patellar tendon-bone allograft. Journal of Orthopaedic Research. 2011;29(8):1193-8.

51. Peters AE, Comerford EJ, Macaulay S, Bates KT, Akhtar R. Micromechanical properties of canine femoral articular cartilage following multiple freeze-thaw cycles. Journal of the Mechanical Behavior of Biomedical Materials. 2017;71:114-21.

52. Müller-Schweinitzer E. Applications for cryopreserved blood vessels in pharmacological research. Cryobiology. 1994;31(1):57-62.

53. Grassl ED, Barocas VH, Bischof JC, editors. Effects of freezing on the mechanical properties of blood vessels. ASME 2004 International Mechanical Engineering Congress and Exposition; 2004: American Society of Mechanical Engineers.

54. Wex C, Stoll A, Fröhlich M, Arndt S, Lippert H. Mechanics of fresh, frozen-thawed and heated porcine liver tissue. International Journal of Hyperthermia. 2014;30(4):271-83.

55. Hukins DWL, Leahy JC, Mathias KJ. Biomaterials: defining the mechanical properties of natural tissues and selection of replacement materials. Journal of Materials Chemistry. 1999;9(3):629-36.

56. Hickey DS, Hukins DWL. Effect of Methods of Preservation on the Arrangement of Collagen Fibrils in Connective Tissue Matrices: An X-Ray Diffraction Study of Annulus Fibrosus. Connect Tissue Research. 1979;6(4):223-8.

57. Müller-Schweinitzer E, Mihatsch M, Schilling M, Haefeli W. Functional recovery of human mesenteric and coronary arteries after cryopreservation at− 196° C in a serum-free medium. Journal of Vascular Surgery. 1997;25(4):743-50.

58. Van Vré EA, Bosmans JM, Van Brussel I, Maris M, De Meyer GRY, Van Schil PE, et al. Immunohistochemical characterisation of dendritic cells in human atherosclerotic lesions: Possible pitfalls. Pathology. 2011;43(3):239-47.

59. Glagov S. Relation of structure to function in arterial walls. Artery. 1979;5(4):295.

60. Fung YC. Biomechanics: mechanical properties of living tissues. New York, NY. 1993.

61. Migneault I, Dartiguenave C, Bertrand MJ, Waldron KC. Glutaraldehyde: behavior in aqueous solution, reaction with proteins, and application to enzyme crosslinking. Biotechniques. 2004;37(5):790-806.

62. Damink LHHO, Dijkstra PJ, Van Luyn MJA, Van Wachem PB, Nieuwenhuis P, Feijen J. Glutaraldehyde as a crosslinking agent for collagen-based biomaterials. Journal of Materials Science: Materials in Medicine. 1995;6(8):460-72.

63. Murtey MD, Ramasamy P. Sample preparations for scanning electron microscopy – life sciences. In: Modern Electron Microscopy in Physical and Life Sciences. Janecek, M (Ed). InTech, 2016.

64. Huang BQ, Yeung EC. Chemical and physical fixation of cells and tissues: an overview. In: Plant Microtechniques and Protocols, Yeung et al. (Eds), Springer, 2015.

65. Fung Y, Sobin S. The retained elasticity of elastin under fixation agents. Journal of Biomechanical Engineering. 1981;103(2):121-2.

66. Mukherjee S, Reddy VJ, Ravichandran R, Mathapati S, Guhathakurta S, Raghunath M, et al., editors. Practical considerations for medical applications using biological grafts and their derivatives. MRS Proceedings; 2012: Cambridge Univ Press.

67. Sung HW, Chang Y, Chiu CT, Chen CN, Liang HC. Crosslinking characteristics and mechanical properties of a bovine pericardium fixed with a naturally occurring crosslinking agent. Journal of Biomedical Materials Research Part A. 1999;47(2):116-26.

68. Chen H, Zhao X, Berwick ZC, Krieger JF, Chambers S, Kassab GS. Microstructure and mechanical property of glutaraldehyde-treated porcine pulmonary ligament. Journal of Biomechanical Engineering. 2016;138(6):061003.

69. Radjeman A, Lim KO. The effect of temperature and glutaraldehyde fixation on the mechanical properties of bovine pericardial tissues. The Japanese Journal of Physiology. 1986;36(6):1093-100.

70. Vesely I. A mechanism for the decrease in stiffness of bioprosthetic heart valve tissues after cross-linking. ASAIO journal. 1996;42(6):993-9.

71. Reichlin T, Wild A, Dürrenberger M, Daniels A, Aebi U, Hunziker PR, et al. Investigating native coronary artery endothelium in situ and in cell culture by scanning force microscopy. Journal of Structural Biology. 2005;152(1):52-63.

72. Pearson B, Espino DM. Effect of hydration on the frequency-dependent viscoelastic properties of articular cartilage. Proceedings of the Institution of Mechanical Engineers, Part H: Journal of Engineering in Medicine. 2013;227(11):1246-52.

73. Xu J, Zhu P, Morris MD, Ramamoorthy A. Solid-state NMR spectroscopy provides atomic-level insights into the dehydration of cartilage. The Journal of Physical Chemistry B. 2011;115(33):9948.

74. Holman BF, Cuplov V, Millner L, Hutton BF, Maher TM, Groves AM, et al. Improved correction for the tissue fraction effect in lung PET/CT imaging. Physics in Medicine and Biology. 2015;60(18):7387-402.

75. Schned AR, Wheeler KJ, Hodorowski CA, Heaney JA, Ernstoff MS, Amdur RJ, et al. Tissue-shrinkage correction factor in the calculation of prostate cancer volume. American Journal of Surgical Pathology. 1996;20(12):1501-6.

76. Angiero F, Parma L, Crippa R, Benedicenti S. Diode laser (808 nm) applied to oral soft tissue lesions: A retrospective study to assess histopathological diagnosis and evaluate physical damage. Lasers in Medical Science. 2012;27(2):383-8.

77. Fick JM. How the structural integrity of the matrix can influence the microstructural response of articular cartilage to compression. Connective Tissue Research. 2013;54(2):83-93..

78. Timmins LH, Wu Q, Yeh AT, Moore JE, Greenwald SE. Structural inhomogeneity and fiber orientation in the inner arterial media. American Journal of Physiology-Heart and Circulatory Physiology. 2010;298(5):H1537-H45.

79. Chiastra C, Gallo D, Tasso P, Iannaccone F, Migliavacca F, Wentzel JJ, et al. Healthy and diseased coronary bifurcation geometries influence near-wall and intravascular flow: A computational exploration of the hemodynamic risk. Journal of Biomechanics. 2017;58(1):79-88.

80. Lee J, Smith NP. The multi-scale modelling of coronary blood flow. Annals of Biomedical Engineering. 2012;40(11):2399-413.

81. Purslow PP, Wess TJ, Hukins DWL. Collagen orientation and molecular spacing during creep and stress-relaxation in soft connective tissues. Journal of Experimental Biology. 1998;201(1):135-42.

82. Dahl SLM, Koh J, Prabhakar V, Niklason LE. Decellularized native and engineered arterial scaffolds for transplantation. Cell Transplantation. 2003;12(6):659-66.

83. Chen L, Han D, Jiang L. On improving blood compatibility: from bioinspired to synthetic design and fabrication of biointerfacial topography at micro/nano scales. Colloids and Surfaces B: Biointerfaces. 2011;85(1):2-7.

84. Fan H, Chen P, Qi R, Zhai J, Wang J, Chen L, et al. Greatly improved blood compatibility by microscopic multiscale design of surface architectures. Small. 2009;5(19):2144-8.

85. Chen H, Cornwell J, Zhang H, Lim T, Resurreccion R, Port T, et al. Cardiac-like flow generator for long-term imaging of endothelial cell responses to circulatory pulsatile flow at microscale. Lab on a Chip. 2013;13(15):2999-3007.

86. Ghosh S, Bowen J, Jiang K, Espino DM, Shepherd DET. Investigation of techniques for the measurement of articular cartilage surface roughness. Micron. 2013;44:179-84.

Tables

Table 1 – Buffer and fixative preparation protocols.

Preparation	Add ingredients	Add solutions and adjust to pH 7.3	Dissolve in distilled water and adjust to 1000 ml	Dissolve in distilled water and adjust to 1000 ml

Buffer/fixative	Total volume	Solutes/Solutions	Supplier	Amount
$NaH_2PO_4 \bullet H_2O$ aq.	1000 ml	$NaH_2PO_4 \bullet H_2O$	Sigma Aldrich, St Louis, MO, USA	27.6 g
$Na_2HPO_4 \bullet 2H_2O$ aq	1000 ml	$Na_2HPO_4 \bullet 2H_2O$	Sigma Aldrich, St Louis, MO, USA	35.61 g
Sodium phosphate buffer solution (0.2 M)	100 ml	$NaH_2PO_4 \bullet H_2O$ aq.		23 ml
		$Na_2HPO_4 \bullet 2H_2O$ aq		77 ml
3% glutaraldehyde	100 ml	Glutaraldehyde (50%)	Fluka Analytical, Sigma Aldrich, St Louis, MO, USA	6 ml
		Sodium phosphate buffer solution (0.2 M)		94 ml

Table 2 – Surface roughness and dimensions (mean, median and standard deviation, SD) of samples at their original state (stage 1), and following a subsequent freeze-thaw cycle (stage 2), glutaraldehyde based fixation (stage 3) and a final dehydration stage (stage 4). Measurements were obtained from six independent specimens. Where † indicates a significant difference for stage 4 as compared to stages 1 and 2, and ‡ indicates a significant difference at stage 4 as compared to stage 3 ($p < 0.05$). Note, $Ra_{cб}$ is the correction following the cumulative processes up to stage 4, for Ra_c.

	Stage 1			Stage 2			Stage 3			Stage 4		
	Mean	Median	SD	Mean	Median	SD	Mean	Median	SD	Mean	Median	SD
Ra_C (µm)	1.36	1.40	0.27	1.28	1.38	0.34	1.49	1.33	0.49	1.98†	2.07	0.26
Ra_L (µm)	0.87	0.76	0.30	1.00	0.91	0.38	1.03	0.75	0.55	1.07	1.08	0.18
L (mm)	1.98	1.98	0.11	1.91	1.95	0.16	1.83	1.82	0.13	1.56†‡	1.56	0.14
W_1 (mm)	0.71	0.69	0.07	0.67	0.67	0.02	0.62	0.62	0.05	0.55†	0.52	0.08
W_2 (mm)	0.58	0.57	0.08	0.57	0.58	0.06	0.53	0.55	0.06	0.43†	0.45	0.06
t (mm)	0.04	0.04	0.01	0.03	0.03	0.01	0.04	0.04	0.01	0.04	0.04	0.01
$Ra_{cб}$ (µm)	1.31	1.42	0.21									

Figure Captions

Figure 1 – *LAD artery samples (a) dissected to reveal its endothelial layer; longitudinal and circumferential orientations are highlighted. (b) Length (L) and sample width (W_1 and W_2) of medial LAD coronary artery specimens used in this study. Note, thickness (t) was measured perpendicular to the x-y plane.*

Figure 2 – Flow chart for processing and imaging stages of LAD coronary artery specimens of porcine hearts (n = 6), frozen immediately after excision.

Figure 3 – Three-dimensional reconstruction of imaged samples (a) in their initial state (stage 1), and following (b) a subsequent freeze-thaw cycle (stage 2), (c) glutaraldehyde fixation (stage 3), and (d) a final dehydration stage (stage 4).

Figure 4 – Optical image of the LAD coronary artery surface (a) at their original state (stage 1), and following a subsequent (b) freeze-thaw cycle (stage 2), (c) glutaraldehyde fixation (stage 3), and (d) a final dehydration stage (stage 4). Axes along which Ra_C and Ra_L measurements were taken are shown.

Figure 5 – Sample surface roughness measurements for Ra_C (top) and Ra_L (bottom).

Figure 6 – Surface roughness mean with 95% confidence intervals (n = 6) at various processing stages (Ra_C – black; Ra_L – white), where process 1 = original, 2 = post-freeze; 3 = post-fixation; 4 = post-dehydration (see Figure 2).

Figr-1

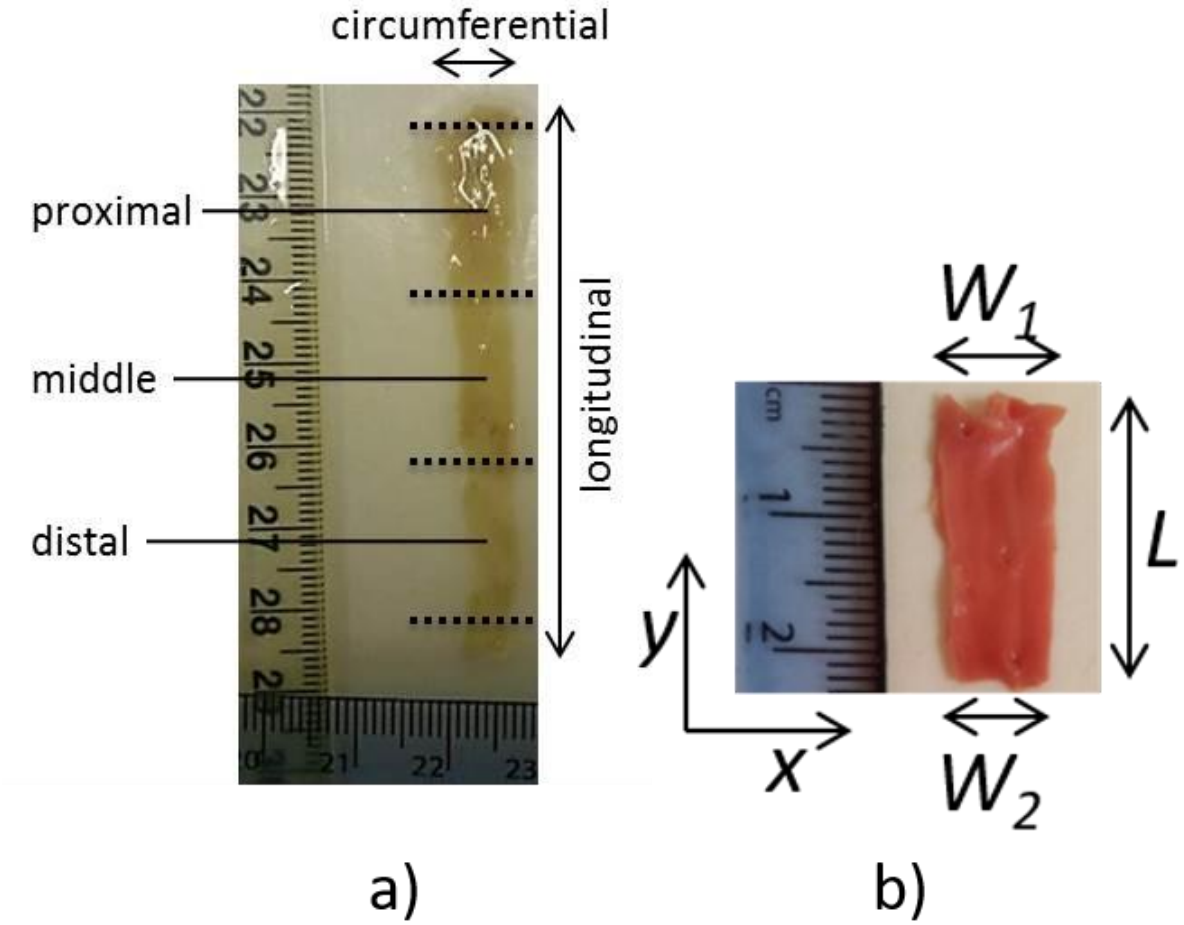

Figr-2

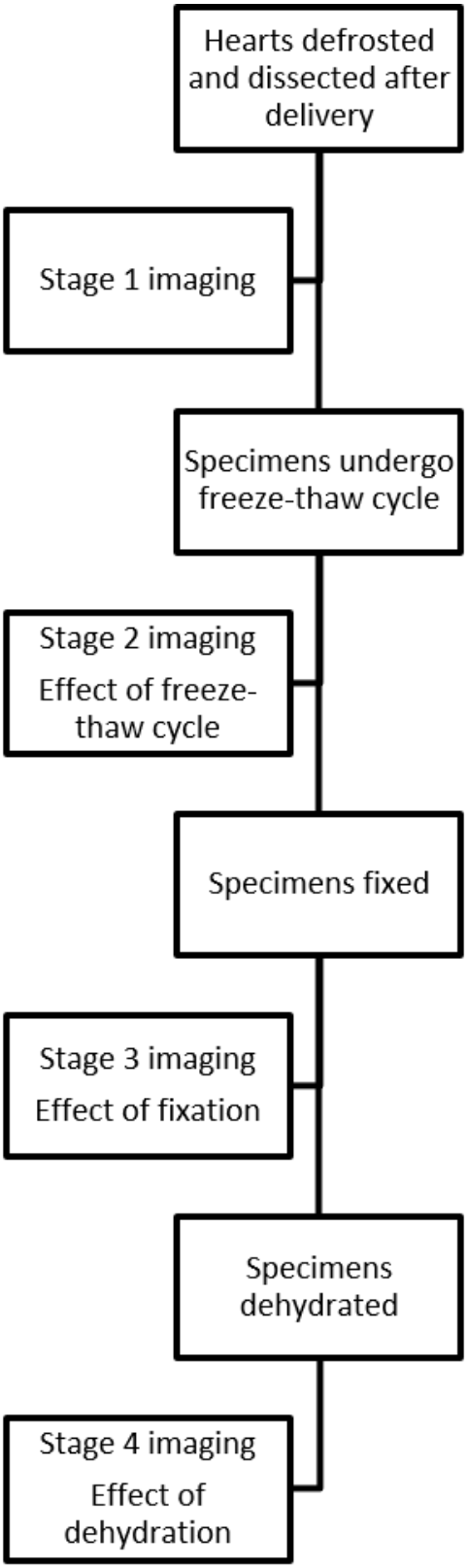

Figr-3

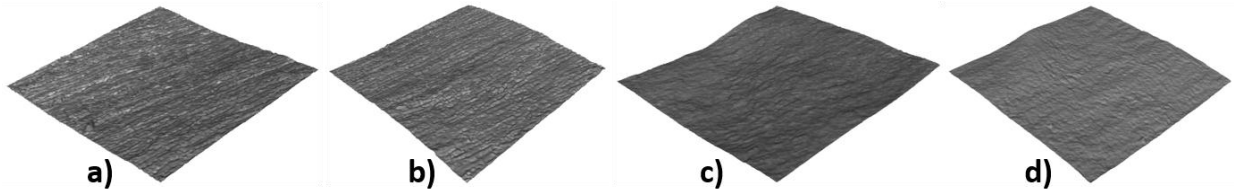

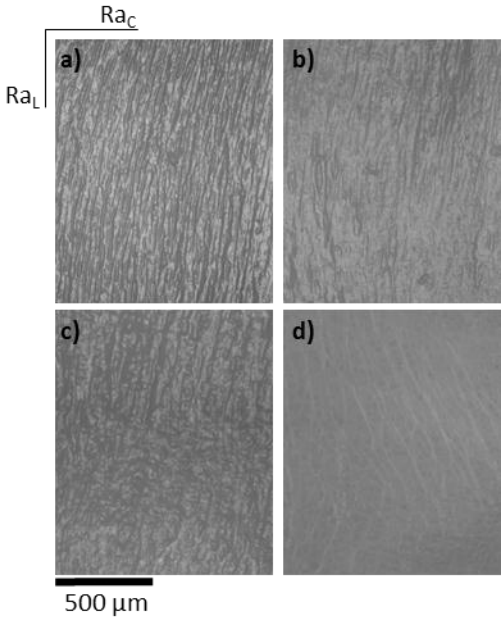

Figr-4

Figr-5

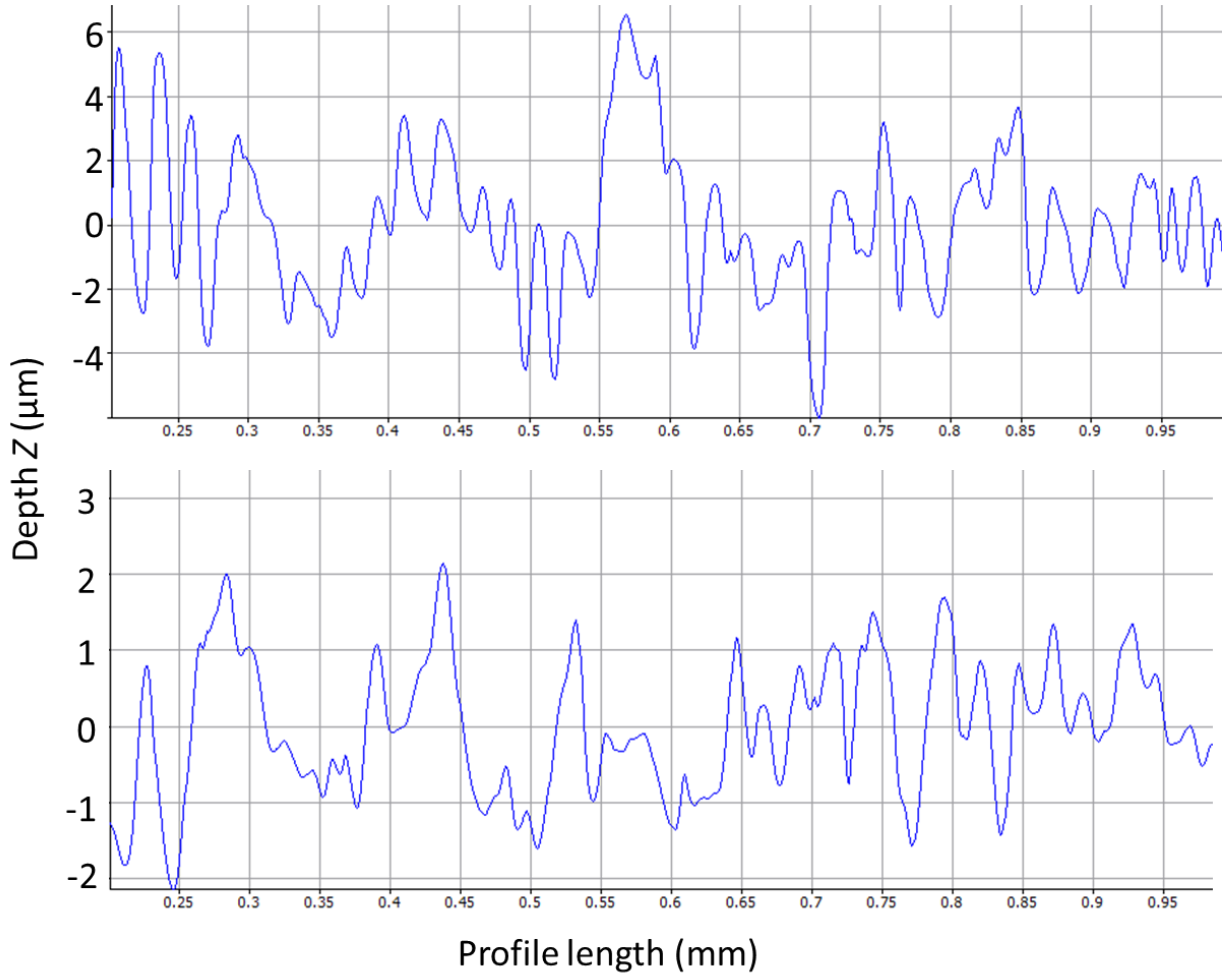

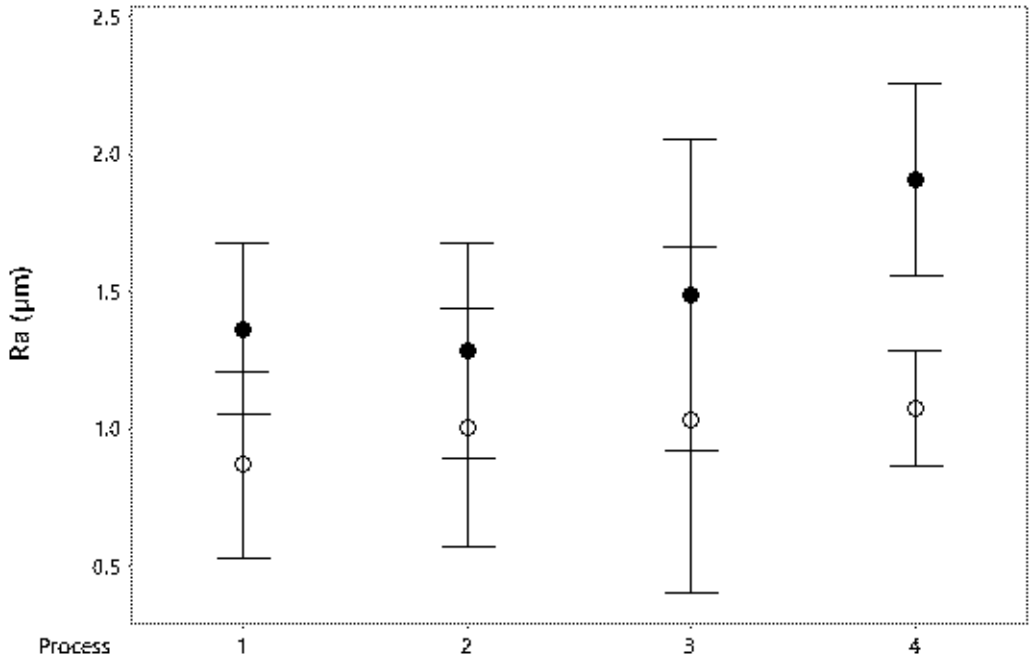

Figr-6